Microwave transmission through an artificial atomic chain coupled to a superconducting photonic crystal

Guo-Zhu Song,[1] Leong-Chuan Kwek,[2,3,4,5] Fu-Guo Deng,[6,7] and Gui-Lu Long[1,8,9,*]

[1]*State Key Laboratory of Low-Dimensional Quantum Physics and Department of Physics, Tsinghua University, Beijing 100084, China*
[2]*Centre for Quantum Technologies, National University of Singapore, 3 Science Drive 2, Singapore 117543, Singapore*
[3]*Institute of Advanced Studies, Nanyang Technological University, Singapore 639673, Singapore*
[4]*National Institute of Education, Nanyang Technological University, Singapore 637616, Singapore*
[5]*MajuLab, CNRS-UNS-NUS-NTU International Joint Research Unit, UMI 3654, Singapore*
[6]*Department of Physics, Applied Optics Beijing Area Major Laboratory, Beijing Normal University, Beijing 100875, China*
[7]*NAAM-Research Group, Department of Mathematics, Faculty of Science, King Abdulaziz University, P.O. Box 80203, Jeddah 21589, Saudi Arabia*
[8]*Tsinghua National Laboratory of Information Science and Technology, Beijing 100084, China*
[9]*Collaborative Innovation Center of Quantum Matter, Beijing 100084, China*

(Received 7 January 2019; revised manuscript received 11 March 2019; published 23 April 2019)

Emitters strongly coupled to a photonic crystal provide a powerful platform for realizing novel quantum light-matter interactions. Here we study the optical properties of a three-level artificial atomic chain coupled to a one-dimensional superconducting microwave photonic crystal. A sharp minimum-energy dip appears in the transmission spectrum of a weak input field, which reveals rich behavior of the long-range interactions arising from localized bound states. We find that the dip frequency scales linearly with both the number of the artificial atoms and the characteristic strength of the long-range interactions when the localization length of the bound state is sufficiently large. Motivated by this observation, we present a simple model to calculate the dip frequency with system parameters, which agrees well with the results from exact numerics for large localization lengths. We observe oscillation between bunching and antibunching in photon-photon correlation function of the output field. Furthermore, we find that the model remains valid even though the coupling strengths between the photonic crystal and artificial atoms are not exactly equal and the phases of external driving fields for the artificial atoms are different. Thus we may infer valuable system parameters from the dip location in the transmission spectrum, which provides an important measuring tool for the superconducting microwave photonic crystal systems in experiment. With remarkable advances to couple artificial atoms with microwave photonic crystals, our proposal may be experimentally realized in currently available superconducting circuits.

DOI: 10.1103/PhysRevA.99.043830

I. INTRODUCTION

In recent years, one-dimensional (1D) waveguide quantum electrodynamics (QED) systems have emerged as an exciting frontier in quantum information science [1–13]. The waveguide systems benefit from the confinement of continuous electromagnetic modes over a large bandwidth, which couple to nearby atoms or embedded artificial atoms. There are a wide variety of systems that can act as waveguide platforms such as plasmonic nanowires [14–17], optical nanofibers [18–34], diamond waveguides [35–38], superconducting transmission lines [39–48], and photonic crystal waveguides [49]. Due to the intrinsically tailorable band structure, photonic crystal waveguides are of particular interest and enable tunable long-range interactions in many-body systems [50–55].

Photonic crystals are highly dispersive periodic dielectric media in which the refractive index is modulated periodically due to photonic band gaps [49,56]. In this configuration, when a qubit trapped nearby the photonic crystal is excited at a frequency inside the band gap, it cannot radiate into the dielectric but gives rise to a qubit-photon bound state [57–62]. The photonic component of the bound state is an exponentially decaying envelope spatially centered at the qubit position, which facilitates coherent excitation exchange with proximal qubits [51,52]. Although significant progress has been made [63–79], realizing efficient coupling in the optical regime faces the challenging task of interfacing emitters with photonic crystal waveguides. Recently, superconducting quantum circuits provide an alternative approach to study the physics of the bound state in the microwave regime [45]. Using a stepped-impedance microwave photonic crystal and a superconducting transmon qubit, Liu *et al.* first experimentally observed the bound state in superconducting transmission lines [80]. In their device, by adjusting the detuning between the qubit and the band edge, the localization length of the bound state is widely tunable. Later, Sundaresan *et al.* experimentally realize strong coupling between two transmon qubits and a superconducting microwave photonic crystal, which is a promising benchmark to create 1D chains of qubit-photon bound states with tunable long-range interactions [81].

Inspired by these remarkable advances, we study here the scattering properties of a weak incident field traveling through

*Corresponding author: gllong@tsinghua.edu.cn

an array of Δ-type artificial atoms coupled to a superconducting microwave photonic crystal. In this work, one transition of the Δ-type artificial atom is inside the band gap, which gives rise to the bound state. Besides, another transition is coupled to the electromagnetic modes of the superconducting microwave photonic crystal, and is utilized to explore the long-range interactions arising from the bound states.

With an effective non-Hermitian Hamiltonian, we calculate the transmission spectrum of a weak microwave input field and observe a sharp minimum-energy dip. We analyze the relation between the dip frequency and the system parameters, such as the number of the artificial atoms and the characteristic strength of the long-range interactions. The results reveal that the dip frequency scales linearly with both the number of the artificial atoms and the characteristic strength for large localization lengths of the bound states, which may provide an important measuring tool for the superconducting microwave photonic crystal systems. Motivated by this observation, we give a simple model to calculate the dip frequency with system parameters. We find that, when the localization length of the bound state is large enough, the results of our model agree well with exact numerics. We also study the photon-photon correlation function in the resonant case, and observe oscillation between bunching and antibunching for both transmitted and reflected fields. Moreover, we study the effects of a Gaussian inhomogeneous broadening of the coupling strength and different phases of the external driving field for the artificial atoms on the dip frequency, respectively. The results show that our model remains valid even though the coupling strengths between the photonic crystal and artificial atoms are not exactly equal and the phases of the driving fields for the artificial atoms are different. That is, in experiment, one may infer the system parameters by measuring the dip frequency in the transmission spectrum.

This article is organized as follows. In Sec. II, we present the physics of an artificial atomic chain coupled to a superconducting microwave photonic crystal, and an effective Hamiltonian is introduced for the system. In Sec. III, we study the transmission spectrum of the weak microwave coherent field and give a simple model to estimate the dip frequency with system parameters. We also calculate the photon-photon correlation function of the output field in the resonant case. Moreover, we analyze the effects of the inhomogeneous broadening of the coupling strength, different phases of the driving field for the artificial atoms, and the dissipation of the bound states on the dip frequency, respectively. In Sec. IV, we discuss the feasibility of our system with recent experiments. Finally, we summarize the results, and discuss the advantage of the superconducting microwave photonic crystal systems in Sec. V.

II. MODEL AND HAMILTONIAN

We model an array of Δ-type artificial atoms coupled to an infinite superconducting microwave photonic crystal, as shown in Fig. 1(a). The superconducting microwave photonic crystal is implemented by periodically alternating sections of low and high impedance coplanar waveguides, which can be realized via changing the gap width and center pin of the coplanar waveguide [80,81]. The dispersion relation of the guided modes in the superconducting microwave photonic

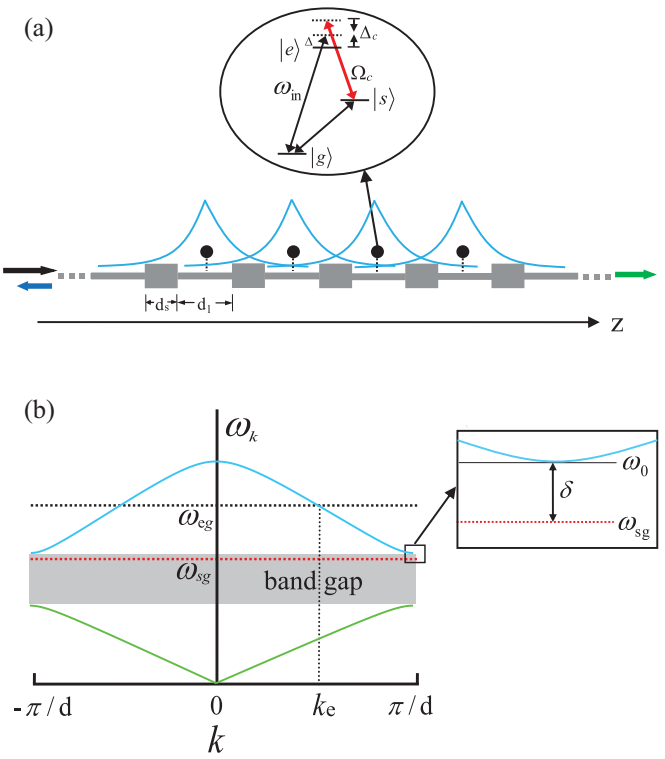

FIG. 1. (a) Schematic diagram of the microwave transport through a three-level artificial atomic chain (black dots) coupled to an infinite superconducting microwave photonic crystal (gray line of alternating width) with unit cell length $d = d_l + d_s$. A coherent microwave field (black arrow) is injected from left to interact with the artificial atomic chain, and then a reflected field (blue arrow) and a transmitted field (green arrow) are collected at the left and right exports, respectively. The blue envelopes represent the photonic components of the bound states, which are spatially centered at the locations of the artificial atoms. (b) Band structure of the 1D superconducting microwave photonic crystal. The green and blue solid lines represent the first and second photonic bands, respectively. The resonance frequency ω_{sg} (horizontal red dashed line) is inside the band gap (gray region) and is close to the second band edge frequency ω_0 with detuning $\delta = \omega_0 - \omega_{sg}$. The resonance frequency ω_{eg} (horizontal black dashed line) lies in the second band and the corresponding wave vector is k_e.

crystal can be obtained by the transfer matrix method [80] and is given by

$$\cos(kd) = \cos\left(\frac{\omega_k d}{v_g}\right) - \frac{1}{2}\left(\frac{Z_l}{Z_s} + \frac{Z_s}{Z_l} - 2\right) \times \sin\left(\frac{\omega_k d_l}{v_g}\right)\sin\left(\frac{\omega_k d_s}{v_g}\right), \quad (1)$$

where k is Bloch wave vector, $d = d_l + d_s$ is the unit cell length, and ω_k is the guided mode frequency with phase velocity v_g. Z_l (Z_s) and d_l (d_s) represent the impedance and length of the high (low) impedance coplanar waveguide in the unit cell, respectively. Each artificial atom has three energy levels $|g\rangle$, $|e\rangle$, and $|s\rangle$. The Δ-type artificial atom can be realized by a flux-based superconducting quantum circuit when the external magnetic flux through the loop $\Phi_e \neq \Phi_0/2$, where Φ_0 is the flux quantum [82,83]. Since the second band is smoother than the first one, each artificial atom is purposely placed in

the center of the high-impedance section, which maximizes (minimizes) the coupling between the artificial atom and the second (first) band [80,81]. Moreover, the width of the second band can be sufficiently large so that the influence of the other band is ignored. In detail, the Δ-type artificial atom is coupled to the high-impedance section of the unit cell through the loop-line mutual inductance M.

Here, we assume that the resonance frequency ω_{sg} of the transition $|g\rangle \leftrightarrow |s\rangle$ is inside the band gap, and is close to second band edge frequency ω_0 with detuning $\delta = \omega_0 - \omega_{sg}$, as shown in Fig. 1(b). In this domain, due to the van Hove singularity in the density of states, the transition $|g\rangle \leftrightarrow |s\rangle$ of the artificial atom is predominantly coupled to the modes close to the second band edge. In this case, we can approximate the dispersion relation near the second band edge to be quadratic $\omega_k \approx \omega_0 + \alpha d^2(k-k_0)^2$, where α denotes the curvature of the band structure and $k_0 = \pi/d$ is the band edge wave vector. Once such an artificial atom is excited to the state $|s\rangle$, a localized bound state appears [51]. Specifically, as shown in Fig. 1(a), in real space, the photonic component of the bound state is exponentially localized around the artificial atom with localization length L, which mediates long-range coherent dipole-dipole interactions with proximal artificial atoms. Since $L \propto \sqrt{1/\delta}$, we can tune the localization length by altering the detuning between the resonance frequency ω_{sg} and the second band edge frequency ω_0.

While it is not allowed to probe this coherent interaction using the input field around frequency ω_{sg} due to the existence of the band gap, thus we assume that the resonance frequency ω_{eg} of the transition $|g\rangle \leftrightarrow |e\rangle$ lies in the second band, which gives rise to the coupling between the transition $|g\rangle \leftrightarrow |e\rangle$ and the modes of the second band. Here, the coupling strengths between all artificial atoms and the second band are assumed to be identical. The single-atom coupling strength to the second band is given by g, where $g \propto MI_p$, with I_p being the amplitude of the persistent current in the loop. That is, we can use the second photonic band as a conventional superconducting transmission line to collect the scattered fields and explore the long-range interactions between the artificial atoms. In addition, with a magnetic flux coil, we introduce an external microwave field (Rabi frequency Ω_c) to drive the transition $|e\rangle \leftrightarrow |s\rangle$ of each artificial atom. In fact, the transition $|e\rangle \leftrightarrow |s\rangle$ driven by an external field connects the two mechanisms mentioned above, i.e., the long-range interactions produced by the transition $|g\rangle \leftrightarrow |s\rangle$ and the detecting channel arising from the coupling between the transition $|g\rangle \leftrightarrow |e\rangle$ and the second band.

The system composed of the artificial atomic chain and the superconducting microwave photonic crystal can be described by an effective non-Hermitian Hamiltonian [51,75,81,84]:

$$
\begin{aligned}
H_{\rm non} = &-\sum_j^n \big[(\Delta + i\Gamma_e^{'}/2)\sigma_{ee}^j + (\Delta - \Delta_c + i\Gamma_s^{'}/2)\sigma_{ss}^j \\
&+ \Omega_c(\sigma_{es}^j + \text{H.c.})\big] - i\frac{\Gamma_0}{2}\sum_{j,k}^n e^{ik_e|z_j - z_k|}\sigma_{eg}^j\sigma_{ge}^k \\
&- V\sum_{j,k}^n (-1)^{|z_j - z_k|/d} e^{-|z_j - z_k|/L}\sigma_{sg}^j\sigma_{gs}^k. \qquad (2)
\end{aligned}
$$

Here $\Delta = \omega_{\rm in} - \omega_{eg}$ is the detuning between the frequency $\omega_{\rm in}$ of the input field with wave vector $k_{\rm in}$ and the resonance frequency ω_{eg}. $\Gamma_e^{'}$ ($\Gamma_s^{'}$) is the decay rate of the state $|e\rangle$ ($|s\rangle$) into free space, n is the number of the artificial atoms, and $\Delta_c = \omega_c - \omega_{es}$ denotes the detuning between the frequency ω_c of the external driving field and the frequency ω_{es} of the transition $|e\rangle \leftrightarrow |s\rangle$. $\Gamma_0 = 4\pi g^2/v_g$ is the single-atom spontaneous emission rate into the photonic crystal modes. z_j represents the position of artificial atom j and V characterizes the strength of the long-range coherent interactions arising from the bound states. Note that we include the case $j = k$ in the last term of Eq. (2), which corresponds to the Stark shift experienced by artificial atom j due to its own bound photon.

Here, we mainly focus on the transport properties of a weak coherent probe field propagating through the artificial atomic chain. The corresponding driving part is given by $H_{\rm dr} = \sqrt{\frac{v_g\Gamma_0}{2}}\mathcal{E}\sum_j^n(\sigma_{eg}^j e^{ik_{\rm in}z_j} + \text{H.c.})$, where $\mathcal{E}$ is the amplitude of the weak probe field (Rabi frequency $\sqrt{\frac{v_g\Gamma_0}{2}}\mathcal{E}$). As a consequence, the dynamics of the system is governed by the total Hamiltonian $H = H_{\rm non} + H_{\rm dr}$ and the initial state is the ground state $|\psi_0\rangle = |g\rangle^{\otimes n}$ of the artificial atomic chain. When the probe field is sufficiently weak ($\sqrt{\frac{v_g\Gamma_0}{2}}\mathcal{E} \ll \Gamma_e^{'}$), the occurrence of quantum jumps is infrequent and can be neglected [85]. Using the input-output formalism [86], the transmitted (T) and reflected (R) field operators are

$$
\begin{aligned}
a_T(z) &= \mathcal{E}e^{ik_{\rm in}z} + i\sqrt{\frac{\Gamma_0}{2v_g}}\sum_j^n \sigma_{ge}^j e^{ik_e(z-z_j)}, \\
a_R(z) &= i\sqrt{\frac{\Gamma_0}{2v_g}}\sum_j^n \sigma_{ge}^j e^{-ik_e(z-z_j)}. \qquad (3)
\end{aligned}
$$

Consequently, the transmittance T and reflection R of the weak probe field are given by

$$
T = \frac{\langle\psi|a_T^\dagger a_T|\psi\rangle}{\mathcal{E}^2}, \quad R = \frac{\langle\psi|a_R^\dagger a_R|\psi\rangle}{\mathcal{E}^2}, \qquad (4)
$$

where $|\psi\rangle$ represents the steady state.

III. NUMERICAL RESULTS

A. Transmission properties of the input field

Here, we consider the case that $n = 10$ artificial atoms are equally spaced along the 1D infinite superconducting microwave photonic crystal. To minimize the reflection of the input field from the artificial atomic chain, we choose the configuration $k_e d = \pi/2$ [86,87]. As shown in Figs. 2(a) and 2(b), we calculate the transmission spectra of the weak monochromatic coherent input field with localization length $L = 4.1d$ for two choices of characteristic strength V. As illustrated in Fig. 2(a), for $V = 0$ (i.e., a conventional superconducting transmission line), we observe the electromagnetically induced transparency phenomenon in the transmission spectrum, while for $V \neq 0$, such as for the case $V = 2.3\Gamma_0$ shown in Fig. 2(b), some new sharp dips emerge in the transmission spectrum, which arise from the long-range coherent interactions between the artificial atoms.

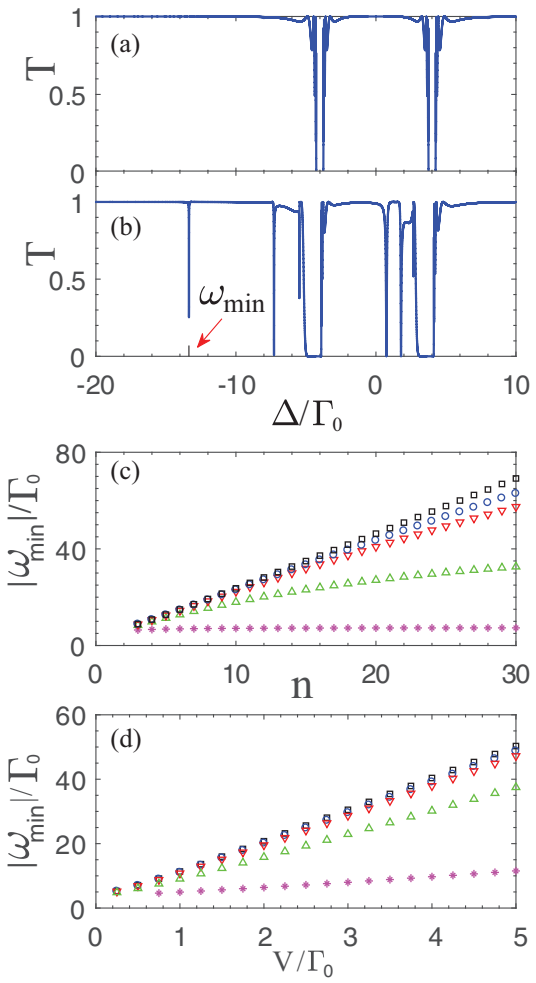

FIG. 2. Transmission spectra of the input field as a function of the frequency detuning Δ/Γ_0 for (a) $V = 0$ and (b) $V = 2.3\Gamma_0$ with localization length $L = 4.1d$ when $n = 10$ artificial atoms are equally spaced along the superconducting microwave photonic crystal. (c) The frequency $|\omega_{\min}|$ versus the number n of the artificial atoms for $L = 10^4 d$ (black squares), $L = 10^2 d$ (blue circles), $L = 50d$ (red down triangles), $L = 10d$ (up green triangles), and $L = d$ (purple asterisks) with $V = 2.3\Gamma_0$. (d) The frequency $|\omega_{\min}|$ as a function of the characteristic strength V for $L = 10^4 d$ (black squares), $L = 10^2 d$ (blue circles), $L = 50d$ (red down triangles), $L = 10d$ (up green triangles), and $L = d$ (purple asterisks) with $n = 10$. Parameters: (a)–(d) $\mathcal{E} = 0.0001\sqrt{\frac{\Gamma_0}{2v_g}}$, $k_e d = \pi/2$, $\Delta_c = 0$, $\Omega_c = 4\Gamma_0$, $\Gamma_e' = 9.5 \times 10^{-6}\Gamma_0$, and $\Gamma_s' = 9.5 \times 10^{-6}\Gamma_0$.

In the following, we mainly focus on the minimum resonance frequency $\omega_{\min}$, since it may reveal rich behavior of the long-range interactions. For simplicity, we adopt $|\omega_{\min}|$ instead of $\omega_{\min}$ in our discussions, which does not qualitatively influence the conclusions. As shown in Fig. 2(c), we plot $|\omega_{\min}|$ as a function of the number n of the artificial atoms coupled to the photonic crystal for different choices of the localization length L. The results show that, in the case $L/d \gg 1$, $|\omega_{\min}|$ scales linearly with the number of the artificial atoms. In particular, for infinite-range interaction such as $L/d = 10^4$, we conclude the relation $|\omega_{\min}| \approx nV$. In fact, by diagonalizing the last term of Eq. (2) for $L/d \to \infty$, we obtain $(n-1)$ degenerate resonance energies zero and one resonance energy $-nV$, while, for finite-range interaction such as $L/d = 10$, the frequency $|\omega_{\min}|$ scales sublinearly with the number of artificial atoms. Moreover, for short-range interaction such as $L = d$, the frequency $|\omega_{\min}|$ almost remains constant despite the fact that we increase the number of the superconducting artificial atoms, as shown in Fig. 2(c). In addition, we also give the frequency $|\omega_{\min}|$ versus the characteristic strength V for different choices of the localization length L. Figure 2(d) reveals that the frequency $|\omega_{\min}|$ scales linearly with the characteristic strength V in all cases.

The above observation motivates us to present a simple model for estimating the frequency $|\omega_{\min}|$ with the parameters V, L, and n. As shown in Figs. 2(a) and 2(b), the minimum resonance energy $\omega_{\min}$ arises from the long-range interaction Hamiltonian

$$H_b = -V\sum_{j,k}^{n} e^{-|z_j - z_k|/L}\sigma_{sg}^{j}\sigma_{gs}^{k}. \tag{5}$$

Here, for brevity, we have ignored the phase factor, which does not qualitatively change the conclusions. Intuitively, for any two atoms j and k chosen from n artificial atoms, we may sum over all possible cases for separations, and get one energy A, i.e.,

$$A = -V\sum_{l=0}^{n-1} e^{-ld/L}. \tag{6}$$

Note that here we include the term $l = 0$, which corresponds to Stark shift experienced by an artificial atom due to its own bound photon. Summing all the terms, we easily obtain

$$|A| = V\frac{e^{d/L} - e^{-(n-1)d/L}}{e^{d/L} - 1}. \tag{7}$$

The result of this model agrees well with the exact numerics shown in Fig. 2(d). That is, the frequency $|\omega_{\min}|$ calculated from exact numerics scales linearly with the characteristic strength V for a fixed number of the artificial atoms and localization length L of the bound states. In the limit $L \gg nd$, using the approximation $e^x \approx (1 + x)$ when $x \to 0$, the energy $|A|$ in Eq. (7) can be written approximately as

$$|A| \approx nV. \tag{8}$$

It is consistent with the result $|\omega_{\min}| \approx nV$ by diagonalizing the long-range interaction Hamiltonian for the infinite localization length mentioned above. Consequently, with this model, in the limit $L \gg d$, we may use the energy $|A|$ to estimate the frequency $|\omega_{\min}|$ with system parameters L, V, n, and d.

To demonstrate the validity of our model, we compare its results with exact numerics, as shown in Fig. 3(a). We observe that this model agrees well with the exact numerics in the limit $L \gg d$, while for finite localization length L, such as $L = 10d$, there is a difference between the two results, and the frequency $|\omega_{\min}|$ scales sublinearly with the number n of the artificial atoms in both cases. To obtain the validity of the localization length L, we give the results from our model and exact numerics as a function of the localization length L, respectively, as shown in Fig. 3(b). We observe that,

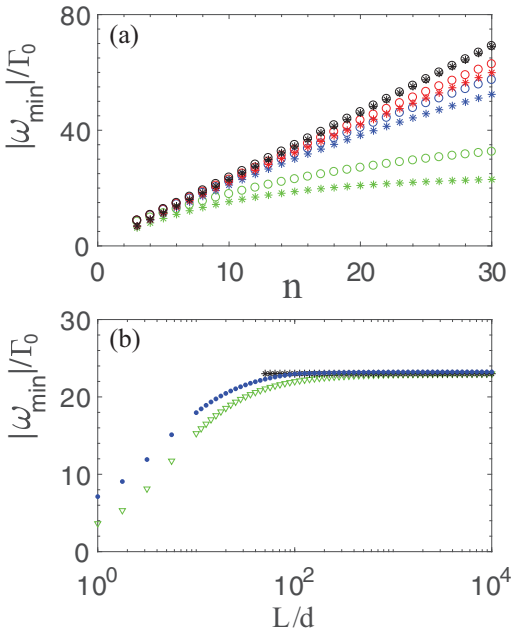

FIG. 3. (a) Frequency $|\omega_{\min}|$ as a function of the number n of the artificial atoms calculated from Eq. (7) (asterisks) and exact numerics (circles) for $L = 10^4 d$ (black), $L = 10^2 d$ (red), $L = 50d$ (blue), and $L = 10d$ (green). (b) The frequency $|\omega_{\min}|$ versus the localization length L calculated from exact numerics (blue dots), Eq. (7) (green down triangles), and Eq. (8) (black asterisks) with $n = 10$. Parameters: (a),(b) $\mathcal{E} = 0.0001\sqrt{\frac{\Gamma_0}{2v_g}}$, $V = 2.3\Gamma_0$, $k_e d = \pi/2$, $\Delta_c = 0$, $\Omega_c = 4\Gamma_0$, $\Gamma_e' = 9.5 \times 10^{-6}\Gamma_0$, and $\Gamma_s' = 9.5 \times 10^{-6}\Gamma_0$.

when $L \geqslant 10^2 d$ in our system, this simple model agrees well with exact numerics. In other words, for a sufficiently large localization length L, one may infer the characteristic strength V of the long-range interactions from Eq. (8) for fixed number of the artificial atoms, by measuring the dip frequency $|\omega_{\min}|$ in the transmission spectrum.

As shown in Fig. 4, with $n = 10$ and five choices of the localization length L, we give the coupling strengths of the nearest and farthest two artificial atoms arising from the long-range coherent interactions in Eq. (5), respectively. For simplicity, here we omit the minus sign in Eq. (5), which does not influence the conclusions. In fact, the interaction strength between two atoms is determined by the overlap of their photonic envelopes with the atoms, as shown in Fig. 1(a). Here, we take the case $j = 1$, $k = 2$ as an example for the nearest two atoms, and $j = 1$, $k = 10$ for the farthest two atoms. The results reveal that, for infinite-range interaction such as $L = 10^4 d$, the interaction strengths for the nearest and farthest two atoms are almost the same, as shown in the second row of Fig. 4. While, when the localization lengths of the bound states decrease gradually, the difference of the interaction strengths between the two cases becomes obvious. Specifically, for short-range interaction such as $L = d$, the interaction strength between the nearest two atoms is approximately $0.37V$, while the interaction between the farthest two atoms becomes very weak and negligible, as shown in the last row of Fig. 4. In other words, for finite localization length L, an atom can only exchange an excitation with proximal atoms through its exponentially decaying envelope of the bound state, but not with the distant atoms. This causes the phenomenon that the minimum resonance energy scales sublinearly with the number n of the artificial atoms for finite localization length, as shown in Fig. 3(a).

L/d	j=1, k=2	j=1, k=10
10000	1.00	1.00
100	0.99	0.91
50	0.98	0.84
10	0.90	0.41
1	0.37	0.00

FIG. 4. Interaction strengths of the nearest two atoms ($j = 1$, $k = 2$) and farthest two atoms ($j = 1$, $k = 10$) arising from Eq. (5) with $n = 10$ for $L = 10^4 d$, $L = 10^2 d$, $L = 50d$, $L = 10d$, and $L = d$. The numbers (in units of V) in the second and third columns retain two digits after the decimal point. Here, we omit the minus sign in Eq. (5).

B. Two-photon correlation

The main feature of nonclassical light is that photons can be bunched or antibunched in time, which is revealed via photon-photon correlation function $g^{(2)}(t)$ (second-order coherence). For a steady state in our system, the photon-photon correlation function $g^{(2)}$ of the output field can be written as

$$g_\alpha^{(2)}(\tau) = \frac{\langle\psi|a_\alpha^\dagger(z)e^{iH\tau}a_\alpha^\dagger(z)a_\alpha(z)e^{-iH\tau}a_\alpha(z)|\psi\rangle}{|\langle\psi|a_\alpha^\dagger(z)a_\alpha(z)|\psi\rangle|^2}, \quad (9)$$

where $\alpha = T, R$ and $|\psi\rangle$ represents the steady-state wave vector.

Now, we turn to discuss the photon-photon correlation function $g^{(2)}(t)$ of the transmitted (reflected) field for two choices of the number n of the artificial atoms in the resonant case ($\Delta = 0$), i.e., $n = 10$ and $n = 20$. Here, $n\Delta$-type artificial atoms are equally spaced along the superconducting microwave photonic crystal. As shown in Fig. 5, we observe oscillation between bunching and antibunching in both $g_T^{(2)}$ and $g_R^{(2)}$ for two cases, i.e., $g^{(2)}$ oscillates around the uncorrelated value 1. Differently, for the transmitted field, initial bunching $[g_T^{(2)}(0) > 1]$ exists and initial antibunching $[g_R^{(2)}(0) = 0]$ is present for the reflected field. By comparing the first and second rows of Fig. 5, we find that the amplitude of the oscillation in $g_R^{(2)}$ is stronger than that in $g_T^{(2)}$ for both $n = 10$ and $n = 20$. The time delay of the oscillation in $g_R^{(2)}$ is longer than that in $g_T^{(2)}$. Moreover, when we increase the number n of the artificial atoms coupled to the photonic crystal, we observe that the oscillation lasts longer in both $g_R^{(2)}$ and $g_T^{(2)}$. This can be concluded by comparing the first and second columns of Fig. 5. The results mentioned above suggest that our system may offer an effective platform to explore the nonclassical light in experiment.

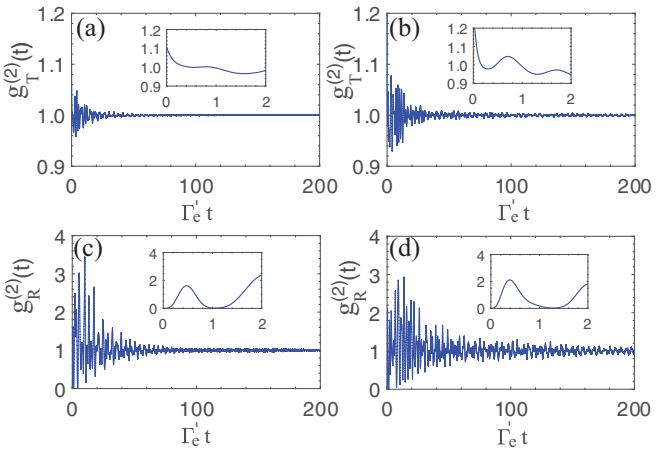

FIG. 5. Photon-photon correlation functions $g_T^{(2)}$ of the transmitted field and $g_R^{(2)}$ of the reflected field in the resonant case $\Delta = 0$ when n artificial atoms are equally spaced along the superconducting microwave photonic crystal. Parameters: (a) and (c) $n = 10$, (b) and (d) $n = 20$; (a)–(d) $\mathcal{E} = 0.0001\sqrt{\frac{\Gamma_0}{2v_g}}$, $V = 2.3\Gamma_0$, $L = 4.1d$, $k_e d = \pi/2$, $\Delta_c = 0$, $\Omega_c = 4\Gamma_0$, $\Gamma_e' = 9.5 \times 10^{-6}\Gamma_0$, and $\Gamma_s' = 9.5 \times 10^{-6}\Gamma_0$.

C. Effects of imperfections

In the above discussions, we have assumed that the coupling strengths between the photonic crystal and artificial atoms are the same, while due to small experimental imperfections, the coupling strengths are not exactly equal in practical condition [81]. Here, we consider that the inhomogeneous broadening of the coupling strength is Gaussian with the probability density $\rho(\delta) = \frac{1}{\sigma\sqrt{2\pi}}\exp(-\frac{\delta^2}{2\sigma^2})$, where δ is the difference value from the expected coupling strength Γ_0 and σ denotes the standard deviation to measure the width of the inhomogeneous broadening. As shown in Fig. 6(a), we give the dip frequency $|\omega_{\min}|$ obtained from exact numerics as a function of the parameter σ. The results show that the frequency $|\omega_{\min}|$ is robust to the inhomogeneous broadening of the coupling strength. In fact, as shown in Figs. 2(a) and 2(b), the frequency $|\omega_{\min}|$ originates from the long-range interaction term in Eq. (2). We conclude that, although the coupling strengths between the photonic crystal and artificial atoms are not exactly equal in experiment, our model is valid.

As mentioned above, the transitions $|e\rangle \leftrightarrow |s\rangle$ of the artificial atoms are driven by external microwave fields. In practical superconducting microwave photonic crystal systems, the phase of the external driving field for each artificial atom may be different, which has been regarded to be identical in the above sections. Here, we assume that the external classical field driving the jth artificial atom has a Rabi frequency Ω_c and a phase ϕ_j, where Ω_c is regarded to be identical for all artificial atoms and ϕ_j is randomly chosen from $[0, \eta]$ in our calculations. As shown in Fig. 6(b), we plot the dip frequency $|\omega_{\min}|$ calculated from exact numerics as a function of the parameter η. Evidently, the dip frequency $|\omega_{\min}|$ is immune to the phase of the external driving field. In other words, our model remains valid even when the phases of the driving field for the artificial atoms are different.

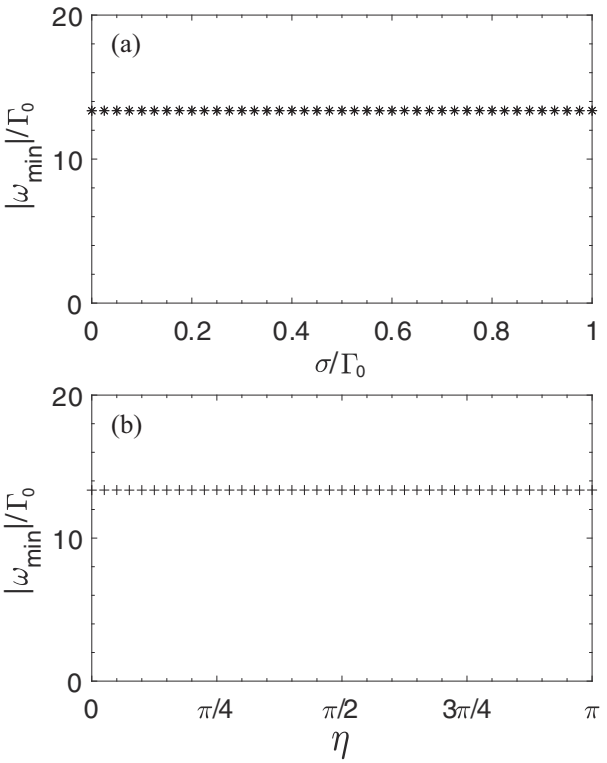

FIG. 6. Frequency $|\omega_{\min}|$ calculated from exact numerics versus the parameters (a) σ and (b) η when $n = 10$ artificial atoms are equally spaced along the superconducting microwave photonic crystal. We average over 10 000 single-shot realizations for each σ (η) with $\mathcal{E} = 0.0001\sqrt{\frac{\Gamma_0}{2v_g}}$, $V = 2.3\Gamma_0$, $L = 4.1d$, $k_e d = \pi/2$, $\Delta_c = 0$, $\Omega_c = 4\Gamma_0$, $\Gamma_e' = 9.5 \times 10^{-6}\Gamma_0$, and $\Gamma_s' = 9.5 \times 10^{-6}\Gamma_0$.

In an infinite superconducting microwave photonic crystal, the bound states can lead to permanent light trapping. However, for a finite system, the dissipation of the bound states exists. Considering this dissipation, the long-range interaction Hamiltonian should be rewritten as

$$H_b' = -\left(V + \frac{i\gamma}{2}\right)\sum_{j,k}^{n}(-1)^{|z_j - z_k|/d} e^{-|z_j - z_k|/L}\sigma_{sg}^{j}\sigma_{gs}^{k}, \quad (10)$$

where γ denotes the dissipation rate of the bound states, assumed to be the same for all the bound states. For an infinite photonic crystal, $\gamma = 0$. For an finite system, γ is proportional to the overlap of the bound states with the edges of the structure, i.e., $\gamma \sim e^{-l/L}$, where l is the length of the system. As shown in Figs. 7(a)–7(c), we calculate the transmission spectra of the incident field for three choices of the dissipation rate, i.e., $\gamma = 0.001\Gamma_0$, $0.01\Gamma_0$, and $0.1\Gamma_0$. We find that the existence of the minimum-energy dip is sensitive to the dissipation rate of the bound states. For example, when we change the rate γ from $0.001\Gamma_0$ to $0.1\Gamma_0$, the dip almost disappears. In addition, to show this phenomenon more clearly, we calculate the transmission T_{dip} at the minimum resonance frequency as a function of the dissipation rate γ, as shown in Fig. 7(d). The results reveal that, to observe the minimum-energy dip, the dissipation of the bound states should be strongly suppressed. In fact, for a realistic superconducting

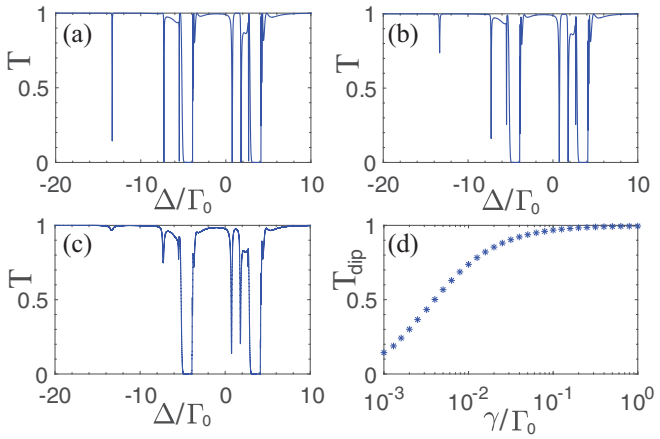

FIG. 7. Transmission spectra of the incident field as a function of the detuning Δ/Γ_0 for (a) $\gamma/\Gamma_0 = 0.001$, (b) $\gamma/\Gamma_0 = 0.01$, and (c) $\gamma/\Gamma_0 = 0.1$ when $n = 10$ artificial atoms are equally spaced along the superconducting microwave photonic crystal. (d) The transmission $T_{\rm dip}$ at the minimum resonance frequency versus the dissipation rate γ of the bound states. Parameters: (a)–(d) $\mathcal{E} = 0.0001\sqrt{\frac{\Gamma_0}{2v_g}}$, $V = 2.3\Gamma_0$, $L = 4.1d$, $k_e d = \pi/2$, $\Delta_c = 0$, $\Omega_c = 4\Gamma_0$, $\Gamma_e' = 9.5 \times 10^{-6}\Gamma_0$, and $\Gamma_s' = 9.5 \times 10^{-6}\Gamma_0$.

photonic crystal [80,81], the dissipation rate is in the range of $\gamma \simeq [20\ \text{MHz}-120\ \text{MHz}]$. Thus $\gamma/\Gamma_0 \simeq [6.0 \times 10^{-5}-3.6 \times 10^{-4}]$, with which we can observe the minimum-energy dip clearly in the transmission spectrum.

IV. EXPERIMENTAL FEASIBILITY

In this section, we discuss the experimental feasibility of our system. The phenomena and conclusions mentioned above may be verified in recent experiments [80,81]. In their devices, a superconducting microwave photonic crystal can be implemented by periodically alternating sections of low and high impedance coplanar waveguides. In the experiment reported by Sundaresan *et al.* [81], two transmon qubits coupled to a superconducting microwave photonic crystal and widely tunable on-site and interbound state interactions have been realized. In their device, the two coplanar waveguide sections are designed to be $d_l = 7.8$ mm, $Z_l = 124\Omega$ and $d_s = 1.2$ mm, $Z_s = 25\Omega$. Under such conditions, the frequency of the second band edge is $\omega_0/2\pi = 7.8$ GHz and $v_p = 1.248 \times 10^8$ m/s. Each artificial atom is individually tunable in frequency by a local flux bias line and the atomic resonance frequency is adjusted to be $\omega_{sg}/2\pi = 7.73$ GHz. Since $L = d\sqrt{\alpha/\delta}$ (α is the band curvature at the band edge), the localization length $L = 4.1d$ adopted in our simulations can be obtained with $\alpha/2\pi = 1.155$ GHz. In fact, longer-range interactions can be realized by reducing the detuning δ of the artificial atom from the band edge. For example, $L \simeq [3.7d - 22.2d]$ has been reported by Liu *et al.* [80]. In addition, the free space emission rate of the state $|s\rangle$ ($|e\rangle$) is $\Gamma_s'/2\pi = 0.5$ MHz ($\Gamma_e'/2\pi = 0.5$ MHz), and single-atom coupling strength to the second band is $g/2\pi = 0.5275$ GHz. Thus the choices of the parameters in our numerical calculations may be experimentally feasible, except for the case $L = 10^4 d$. In fact, this case ($L = 10^4 d$) is merely chosen as an idealized point of comparison.

Besides the transmon circuits, a Δ-type three-level artificial atom can also be realized by a flux-based superconducting circuit [45]. Thus, to reach the ultrastrong-coupling regime, the transmon in their devices can be replaced by a flux qubit [88,89]. Besides the method shown in the two experiments [80,81], there are other approaches to realize superconducting microwave photonic crystals, such as lumped element circuits and Josephson junction arrays.

V. CONCLUSION

In conclusion, we have studied the transport properties of a Δ-type artificial atomic chain coupled to an infinite superconducting microwave photonic crystal. In this work, we take advantage of the superconducting quantum circuits, which provide widely tunable artificial atoms with long coherence times [90,91]. Here, to reach the strong-coupling or ultrastrong-coupling regimes, the artificial atomic chain can be realized by superconducting transmon qubits [80,81] or flux qubits [82,83,88,89,92].

In our system, we place the resonance frequency ω_{sg} of the transition $|g\rangle \leftrightarrow |s\rangle$ inside the band gap, which gives rise to the long-range coherent dipole-dipole interactions between the artificial atoms. To probe the above mechanism in many-body regime, we utilize the coupling between the atomic transition $|g\rangle \leftrightarrow |e\rangle$ and the second band modes of the superconducting microwave photonic crystal. According to the phenomena concluded from exact numerics, we present a simple model to estimate the dip frequency with known system parameters. The results reveal that our model agrees well with exact numerics when the localization length is sufficiently large. We also calculate the photon-photon correlation function of the output field, and observe oscillation between bunching and antibunching for both transmitted and reflected fields. Moreover, we analyze the influence of a Gaussian inhomogeneous broadening of the coupling strength, different phases of the external driving field for the artificial atoms, and the dissipation of the bound states on the dip frequency, respectively. We show numerically that the above conclusions still hold when the coupling strengths between the photonic crystal and artificial atoms are not exactly equal and the phases of the driving field for the artificial atoms are different in practical conditions. With the dissipation rate of the bound states in a realistic superconducting photonic crystal, we can observe the minimum-energy dip clearly in the transmission spectrum. That is, with our model, one may acquire valuable system parameters by measuring the dip frequency in the transmission spectrum, which opens up a new avenue to explore the superconducting microwave photonic crystal systems.

ACKNOWLEDGMENTS

We would like to thank W. Nie for helpful discussions. This work is supported by the National Natural Science Foundation of China under Grants No. 11175094 and No. 91221205, and the China Postdoctoral Science Foundation under Grant No. 2017M620732. L.-C.K. acknowledges support from the National Research Foundation and Ministry of Education, Singapore. F.-G.D. is supported by the National Natural

Science Foundation of China under Grant No. 11674033. G.-L.L. acknowledges support from the Center of Atomic and Molecular Nanosciences, Tsinghua University, and Beijing Advanced Innovation Center for Future Chip (ICFC).

[1] J. T. Shen and S. Fan, Coherent photon transport from spontaneous emission in one-dimensional waveguides, Opt. Lett. **30**, 2001 (2005).

[2] J. T. Shen and S. Fan, Strongly Correlated Two-Photon Transport in a One-Dimensional Waveguide Coupled to a Two-Level System, Phys. Rev. Lett. **98**, 153003 (2007).

[3] J. T. Shen and S. Fan, Theory of single-photon transport in a single-mode waveguide. I. Coupling to a cavity containing a two-level atom, Phys. Rev. A **79**, 023837 (2009).

[4] S. Fan, Ş. E. Kocabaş, and J. T. Shen, Input-output formalism for few-photon transport in one-dimensional nanophotonic waveguides coupled to a qubit, Phys. Rev. A **82**, 063821 (2010).

[5] L. Zhou, L. P. Yang, Y. Li, and C. P. Sun, Quantum Routing of Single Photons with a Cyclic Three-Level System, Phys. Rev. Lett. **111**, 103604 (2013).

[6] P. Lodahl, S. Mahmoodian, and S. Stobbe, Interfacing single photons and single quantum dots with photonic nanostructures, Rev. Mod. Phys. **87**, 347 (2015).

[7] Z. Liao, X. Zeng, H. Nha, and M. S. Zubairy, Photon transport in a one-dimensional nanophotonic waveguide QED system, Phys. Scr. **91**, 063004 (2016).

[8] D. Roy, C. M. Wilson, and O. Firstenberg, Strongly interacting photons in one-dimensional continuum, Rev. Mod. Phys. **89**, 021001 (2017).

[9] S. Das, V. E. Elfving, S. Faez, and A. S. Sørensen, Interfacing Superconducting Qubits and Single Optical Photons Using Molecules in Waveguides, Phys. Rev. Lett. **118**, 140501 (2017).

[10] M. T. Manzoni, D. E. Chang, and J. S. Douglas, Simulating quantum light propagation through atomic ensembles using matrix product states, Nat. Commun. **8**, 1743 (2017).

[11] K. Xia, F. Nori, and M. Xiao, Cavity-Free Optical Isolators and Circulators Using a Chiral Cross-Kerr Nonlinearity, Phys. Rev. Lett. **121**, 203602 (2018).

[12] D. E. Chang, J. S. Douglas, A. González-Tudela, C.-L. Hung, and H. J. Kimble, Colloquium: Quantum matter built from nanoscopic lattices of atoms and photons, Rev. Mod. Phys. **90**, 031002 (2018).

[13] Z. H. Chen, Y. Zhou, and J. T. Shen, Entanglement-preserving approach for reservoir-induced photonic dissipation in waveguide QED systems, Phys. Rev. A **98**, 053830 (2018).

[14] A. V. Akimov, A. Mukherjee, C. L. Yu, D. E. Chang, A. S. Zibrov, P. R. Hemmer, H. Park, and M. D. Lukin, Quantum matter built from nanoscopic lattices of atoms and photons, Nature (London) **450**, 402 (2007).

[15] D. E. Chang, A. S. Sørensen, E. A. Demler, and M. D. Lukin, A single-photon transistor using nanoscale surface plasmons, Nat. Phys. **3**, 807 (2007).

[16] A. Gonzalez-Tudela, D. Martin-Cano, E. Moreno, L. Martin-Moreno, C. Tejedor, and F. J. Garcia-Vidal, Entanglement of Two Qubits Mediated by One-Dimensional Plasmonic Waveguides, Phys. Rev. Lett. **106**, 020501 (2011).

[17] G. M. Akselrod, C. Argyropoulos, T. B. Hoang, C. Ciracì, C. Fang, J. Huang, D. R. Smith, and M. H. Mikkelsen, Probing the mechanisms of large Purcell enhancement in plasmonic nanoantennas, Nat. Photon. **8**, 835 (2014).

[18] B. Dayan, A. S. Parkins, T. Aoki, E. P. Ostby, K. J. Vahala, and H. J. Kimble, A photon turnstile dynamically regulated by one atom, Science **319**, 1062 (2008).

[19] E. Vetsch, D. Reitz, G. Sagué, R. Schmidt, S. T. Dawkins, and A. Rauschenbeutel, Optical Interface Created by Laser-Cooled Atoms Trapped in the Evanescent Field Surrounding an Optical Nanofiber, Phys. Rev. Lett. **104**, 203603 (2010).

[20] S. T. Dawkins, R. Mitsch, D. Reitz, E. Vetsch, and A. Rauschenbeutel, Dispersive Optical Interface Based on Nanofiber-Trapped Atoms, Phys. Rev. Lett. **107**, 243601 (2011).

[21] D. Reitz, C. Sayrin, R. Mitsch, P. Schneeweiss, and A. Rauschenbeutel, Coherence Properties of Nanofiber-Trapped Cesium Atoms, Phys. Rev. Lett. **110**, 243603 (2013).

[22] J. Petersen, J. Volz, and A. Rauschenbeutel, Chiral nanophotonic waveguide interface based on spin-orbit interaction of light, Science **346**, 67 (2014).

[23] F. Le Kien and A. Rauschenbeutel, Anisotropy in scattering of light from an atom into the guided modes of a nanofiber, Phys. Rev. A **90**, 023805 (2014).

[24] R. Mitsch, C. Sayrin, B. Albrecht, P. Schneeweiss, and A. Rauschenbeutel, Quantum state-controlled directional spontaneous emission of photons into a nanophotonic waveguide, Nat. Commun. **5**, 5713 (2014).

[25] B. Gouraud, D. Maxein, A. Nicolas, O. Morin, and J. Laurat, Demonstration of a Memory for Tightly Guided Light in an Optical Nanofiber, Phys. Rev. Lett. **114**, 180503 (2015).

[26] C. Sayrin, C. Clausen, B. Albrecht, P. Schneeweiss, and A. Rauschenbeutel, Storage of fiber-guided light in a nanofiber-trapped ensemble of cold atoms, Optica **2**, 353 (2015).

[27] H. L. Sørensen, J. B. Béguin, K. W. Kluge, I. Iakoupov, A. S. Sørensen, J. H. Müller, E. S. Polzik, and J. Appel, Coherent Backscattering of Light Off One-Dimensional Atomic Strings, Phys. Rev. Lett. **117**, 133604 (2016).

[28] G. Z. Song, Q. Liu, J. Qiu, G. J. Yang, F. Alzahrani, A. Hobiny, F. G. Deng, and M. Zhang, Heralded quantum gates for atomic systems assisted by the scattering of photons off single emitters, Ann. Phys. (NY) **387**, 152 (2017).

[29] P. Solano, P. B. Blostein, F. K. Fatemi, L. A. Orozco, and S. L. Rolston, Super-radiance reveals infinite-range dipole interactions through a nanofiber, Nat. Commun. **8**, 1857 (2017).

[30] M. T. Cheng, J. P. Xu, and G. S. Agarwal, Waveguide transport mediated by strong coupling with atoms, Phys. Rev. A **95**, 053807 (2017).

[31] G. Z. Song, E. Munro, W. Nie, F. G. Deng, G. J. Yang, and L. C. Kwek, Photon scattering by an atomic ensemble coupled to a one-dimensional nanophotonic waveguide, Phys. Rev. A **96**, 043872 (2017).

[32] W. B. Yan, W. Y. Ni, J. Zhang, F. Y. Zhang, and H. Fan, Tunable single-photon diode by chiral quantum physics, Phys. Rev. A **98**, 043852 (2018).

[33] C. H. Yan, Y. Li, H. D. Yuan, and L. F. Wei, Targeted photonic routers with chiral photon-atom interactions, Phys. Rev. A **97**, 023821 (2018).

[34] D. C. Yang, M. T. Cheng, X. S. Ma, J. P. Xu, C. J. Zhu, and X. S. Huang, Phase-modulated single-photon router, Phys. Rev. A **98**, 063809 (2018).

[35] T. M. Babinec, J. M. Hausmann, M. Khan, Y. Zhang, J. R. Maze, P. R. Hemmer, and M. Lončar, A diamond nanowire single-photon source, Nat. Nanotechnol. **5**, 195 (2010).

[36] J. Claudon, J. Bleuse, N. S. Malik, M. Bazin, P. Jaffrennou, N. Gregersen, C. Sauvan, P. Lalanne, and J. M. Gérard, A highly efficient single-photon source based on a quantum dot in a photonic nanowire, Nat. Photon. **4**, 174 (2010).

[37] H. Clevenson, M. E. Trusheim, C. Teale, T. Schröder, D. Braje, and D. Englund, Broadband magnetometry and temperature sensing with a light-trapping diamond waveguide, Nat. Phys. **11**, 393 (2015).

[38] A. Sipahigil, R. E. Evans, D. D. Sukachev, M. J. Burek, J. Borregaard, M. K. Bhaskar, C. T. Nguyen, J. L. Pacheco, H. A. Atikian, C. Meuwly, R. M. Camacho, F. Jelezko, E. Bielejec, H. Park, M. Lončar, and M. D. Lukin, An integrated diamond nanophotonics platform for quantum-optical networks, Science **354**, 847 (2016).

[39] A. Wallraff, D. I. Schuster, A. Blais, L. Frunzio, R. S. Huang, J. Majer, S. Kumar, S. M. Girvin, and R. J. Schoelkopf, Strong coupling of a single photon to a superconducting qubit using circuit quantum electrodynamics, Nature (London) **431**, 162 (2004).

[40] J. T. Shen and S. Fan, Coherent Single Photon Transport in a One-Dimensional Waveguide Coupled with Superconducting Quantum Bits, Phys. Rev. Lett. **95**, 213001 (2005).

[41] L. Zhou, Z. R. Gong, Y. X. Liu, C. P. Sun, and F. Nori, Controllable Scattering of a Single Photon inside a One-Dimensional Resonator Waveguide, Phys. Rev. Lett. **101**, 100501 (2008).

[42] O. Astafiev, A. M. Zagoskin, A. A. Abdumalikov, Y. A. Pashkin, T. Yamamoto, K. Inomata, Y. Nakamura, and J. S. Tsai, Resonance fluorescence of a single artificial atom, Science **327**, 840 (2010).

[43] A. F. van Loo, A. Fedorov, K. Lalumiére, B. C. Sanders, A. Blais, and A. Wallraff, Photon-mediated interactions between distant artificial atoms, Science **342**, 1494 (2013).

[44] K. Lalumière, B. C. Sanders, A. F. van Loo, A. Fedorov, A. Wallraff, and A. Blais, Input-output theory for waveguide QED with an ensemble of inhomogeneous atoms, Phys. Rev. A **88**, 043806 (2013).

[45] X. Gu, A. F. Kockum, A. Miranowicz, Y. X. Liu, and F. Nori, Microwave photonics with superconducting quantum circuits, Phys. Rep. **718-719**, 1 (2017).

[46] A. F. Kockum, G. Johansson, and F. Nori, Decoherence-Free Interaction Between Giant Atoms in Waveguide Quantum Electrodynamics, Phys. Rev. Lett. **120**, 140404 (2018).

[47] M. Mirhosseini, E. Kim, V. S. Ferreira, M. Kalaee, A. Sipahigil, A. J. Keller, and O. Painter, Superconducting metamaterials for waveguide quantum electrodynamics, Nat. Commun. **9**, 3706 (2018).

[48] P. M. Harrington, M. Naghiloo, D. Tan, and K. W. Murch, Bath engineering of a fluorescing artificial atom with a photonic crystal, arXiv:1812.04205.

[49] J. D. Joannopoulos, S. G. Johnson, J. N. Winn, and R. D. Meade, *Photonic Crystals: Molding the Flow of Light*, 2nd ed. (Princeton University Press, Princeton, NJ, 2008).

[50] A. González-Tudela, C. L. Hung, D. E. Chang, J. I. Cirac, and H. J. Kimble, Subwavelength vacuum lattices and atom-atom interactions in two-dimensional photonic crystals, Nat. Photon. **9**, 320 (2015).

[51] J. S. Douglas, H. Habibian, C. L. Hung, A. V. Gorshkov, H. J. Kimble, and D. E. Chang, Quantum many-body models with cold atoms coupled to photonic crystals, Nat. Photon. **9**, 326 (2015).

[52] J. S. Douglas, T. Caneva, and D. E. Chang, Photon Molecules in Atomic Gases Trapped Near Photonic Crystal Waveguides, Phys. Rev. X **6**, 031017 (2016).

[53] E. Munro, L. C. Kwek, and D. E. Chang, Optical properties of an atomic ensemble coupled to a band edge of a photonic crystal waveguide, New J. Phys. **19**, 083018 (2017).

[54] A. González-Tudela and J. I. Cirac, Exotic quantum dynamics and purely long-range coherent interactions in Dirac conelike baths, Phys. Rev. A **97**, 043831 (2018).

[55] G. Z. Song, E. Munro, W. Nie, L. C. Kwek, F. G. Deng, and G. L. Long, Photon transport mediated by an atomic chain trapped along a photonic crystal waveguide, Phys. Rev. A **98**, 023814 (2018).

[56] L. Gan and Z. Y. Li, Photonic crystal cavities and integrated optical devices, Sci. Chin.-Phys. Mech. Astron. **58**, 114203 (2015).

[57] S. John and J. Wang, Quantum Electrodynamics Near a Photonic Band Gap: Photon Bound States and Dressed Atoms, Phys. Rev. Lett. **64**, 2418 (1990).

[58] S. John and J. Wang, Quantum optics of localized light in a photonic band gap, Phys. Rev. B **43**, 12772 (1991).

[59] S. John and T. Quang, Localization of Superradiance near a Photonic Band Gap, Phys. Rev. Lett. **74**, 3419 (1995).

[60] G. Calajó, F. Ciccarello, D. E. Chang, and P. Rabl, Atom-field dressed states in slow-light waveguide QED, Phys. Rev. A **93**, 033833 (2016).

[61] T. Shi, Y.-H. Wu, A. González-Tudela, and J. I. Cirac, Bound States in Boson Impurity Models, Phys. Rev. X **6**, 021027 (2016).

[62] M. Bello, G. Platero, J. I. Cirac, and A. González-Tudela, Unconventional quantum optics in topological waveguide QED, arXiv:1811.04390.

[63] T. Lund-Hansen, S. Stobbe, B. Julsgaard, H. Thyrrestrup, T. Sünner, M. Kamp, A. Forchel, and P. Lodahl, Experimental Realization of Highly Efficient Broadband Coupling of Single Quantum Dots to a Photonic Crystal Waveguide, Phys. Rev. Lett. **101**, 113903 (2008).

[64] A. Laucht, S. Pütz, T. Günthner, N. Hauke, R. Saive, S. Frédérick, M. Bichler, M.-C. Amann, A. W. Holleitner, M. Kaniber, and J. J. Finley, A Waveguide-Coupled On-Chip Single-Photon Source, Phys. Rev. X **2**, 011014 (2012).

[65] J. D. Thompson, T. G. Tiecke, N. P. de Leon, J. Feist, A. V. Akimov, M. Gullans, A. S. Zibrov, V. Vuletić, and M. D. Lukin, Coupling a single trapped atom to a nanoscale optical cavity, Science **340**, 1202 (2013).

[66] A. Goban, C.-L. Hung, S.-P. Yu, J. D. Hood, J. A. Muniz, J. H. Lee, M. J. Martin, A. C. McClung, K. S. Choi, D. E. Chang, O. Painter, and H. J. Kimble, Atom-light interactions in photonic crystals, Nat. Commun. **5**, 3808 (2014).

[67] T. G. Tiecke, J. D. Thompson, N. P. de Leon, L. R. Liu, V. Vuletić, and M. D. Lukin, Nanophotonic quantum phase switch with a single atom, Nature (London) **508**, 241 (2014).

[68] M. Arcari, I. Söllner, A. Javadi, S. Lindskov Hansen, S. Mahmoodian, J. Liu, H. Thyrrestrup, E. H. Lee, J. D. Song, S. Stobbe, and P. Lodahl, Near-Unity Coupling Efficiency of a Quantum Emitter to a Photonic Crystal Waveguide, Phys. Rev. Lett. **113**, 093603 (2014).

[69] S.-P. Yu, J. D. Hood, J. A. Muniz, M. J. Martin, R. Norte, C.-L. Hung, S. M. Meenehan, J. D. Cohen, O. Painter, and H. J. Kimble, Nanowire photonic crystal waveguides for single-atom trapping and strong light-matter interactions, Appl. Phys. Lett. **104**, 111103 (2014).

[70] A. González-Tudela, V. Paulisch, D. E. Chang, H. J. Kimble, and J. I. Cirac, Deterministic Generation of Arbitrary Photonic States Assisted by Dissipation, Phys. Rev. Lett. **115**, 163603 (2015).

[71] A. B. Young, A. C. T. Thijssen, D. M. Beggs, P. Androvitsaneas, L. Kuipers, J. G. Rarity, S. Hughes, and R. Oulton, Polarization Engineering in Photonic Crystal Waveguides for Spin-Photon Entanglers, Phys. Rev. Lett. **115**, 153901 (2015).

[72] A. Goban, C.-L. Hung, J. D. Hood, S.-P. Yu, J. A. Muniz, O. Painter, and H. J. Kimble, Superradiance for Atoms Trapped along a Photonic Crystal Waveguide, Phys. Rev. Lett. **115**, 063601 (2015).

[73] I. Söllner, S. Mahmoodian, S. L. Hansen, L. Midolo, A. Javadi, G. Kiršanskė, T. Pregnolato, H. El-Ella, E. H. Lee, J. D. Song, S. Stobbe, and P. Lodahl, Deterministic photon-emitter coupling in chiral photonic circuits, Nat. Nanotechnol. **10**, 775 (2015).

[74] B. Le Feber, N. Rotenberg, and L. Kuipers, Nanophotonic control of circular dipole emission, Nat. Commun. **6**, 6695 (2015).

[75] J. D. Hood, A. Goban, A. Asenjo-Garcia, M. Lu, S.-P. Yu, D. E. Chang, and H. J. Kimble, Atom-atom interactions around the band edge of a photonic crystal waveguide, Proc. Natl. Acad. Sci. U.S.A. **113**, 10507 (2016).

[76] T. Li, A. Miranowicz, X. Hu, K. Xia, and F. Nori, Quantum memory and gates using a Λ-type quantum emitter coupled to a chiral waveguide, Phys. Rev. A **97**, 062318 (2018).

[77] S.-P. Yu, J. A. Muniz, C.-L. Hung, and H. J. Kimble, Two-dimensional photonic crystals for engineering atom-light interactions, arXiv:1812.08936.

[78] A. González-Tudela and F. Galve, Anisotropic quantum emitter interactions in two-dimensional photonic-crystal baths, ACS Photonics **6**, 221 (2019).

[79] A. P. Burgersa, L. S. Penga, J. A. Muniza, A. C. McClunga, M. J. Martina, and H. J. Kimble, Clocked atom delivery to a photonic crystal waveguide, Proc. Natl. Acad. Sci. U.S.A. **116**, 456 (2019).

[80] Y. Liu and A. A. Houck, Quantum electrodynamics near a photonic bandgap, Nat. Phys. **13**, 48 (2017).

[81] N. M. Sundaresan, R. Lundgren, G. Zhu, A. V. Gorshkov, and A. A. Houck, Interacting Qubit-Photon Bound States with Superconducting Circuits, Phys. Rev. X **9**, 011021 (2019).

[82] Y.-x. Liu, J. Q. You, L. F. Wei, C. P. Sun, and F. Nori, Optical Selection Rules and Phase-Dependent Adiabatic State Control in a Superconducting Quantum Circuit, Phys. Rev. Lett. **95**, 087001 (2005).

[83] W. Z. Jia, Y. W. Wang, and Y.-x. Liu, Efficient single-photon frequency conversion in the microwave domain using superconducting quantum circuits, Phys. Rev. A **96**, 053832 (2017).

[84] D. E. Chang, L. Jiang, A. V. Gorshkov, and H. J. Kimble, Cavity QED with atomic mirrors, New J. Phys. **14**, 063003 (2012).

[85] A. Albrecht, T. Caneva, and D. E. Chang, Changing optical band structure with single photons, New J. Phys. **19**, 115002 (2017).

[86] T. Caneva, M. T. Manzoni, T. Shi, J. S. Douglas, J. I. Cirac, and D. E. Chang, Quantum dynamics of propagating photons with strong interactions: A generalized input-output formalism, New J. Phys. **17**, 113001 (2015).

[87] D. E. Chang, A. H. Safavi-Naeini, M. Hafezi, and O. Painter, Slowing and stopping light using an optomechanical crystal array, New J. Phys. **13**, 023003 (2011).

[88] P. Forn-Díaz, J. J. García-Ripoll, B. Peropadre, J.-L. Orgiazzi, M. A. Yurtalan, R. Belyansky, C. M. Wilson, and A. Lupascu, Ultrastrong coupling of a single artificial atom to an electromagnetic continuum in the nonperturbative regime, Nat. Phys. **13**, 39 (2017).

[89] F. Yoshihara, T. Fuse, S. Ashhab, K. Kakuyanagi, S. Saito, and K. Semba, Superconducting qubit-oscillator circuit beyond the ultrastrong-coupling regime, Nat. Phys. **13**, 44 (2017).

[90] I. Buluta, S. Ashhab, and F. Nori, Natural and artificial atoms for quantum computation, Rep. Prog. Phys. **74**, 104401 (2011).

[91] A. A. Houck, H. E. Türeci, and J. Koch, On-chip quantum simulation with superconducting circuits, Nat. Phys. **8**, 292 (2012).

[92] A. F. Kockum, A. Miranowicz, S. De Liberato, S. Savasta, and F. Nori, Ultrastrong coupling between light and matter, Nat. Rev. Phys. **1**, 19 (2019).